Experimentally Testing a Halbach Rotor Coaxial Magnetic Gear with 279Nm/L Torque Density

Ho Yin (David) Wong, *Student member*, *IEEE*, Hossein Baninajar, *Student member*, *IEEE*,
Bertrand W. Dechant, Parker Southwick, Jonathan Z. Bird, *Member, IEEE*

***Abstract* -- This paper presents the practical design, analysis, and experimental testing results and encountered issues for a 5.67:1 Halbach rotor magnetic gear with a ferromagnetic back support. Testing results for both a Halbach rotor magnetic gear with rectangular modulation supports and a bridgeless circular modulation support rod design is evaluated. The presented magnetic gear design is shown to be capable of operating with a peak torque of 189 Nm and an active region torque density of 279.3Nm/L.**

Index Terms--Magnetic gear, permanent magnet, Halbach array

I. Introduction

A COAXIAL magnetic gear (MG) utilizes magnetic field space modulation to achieve speed-amplification without any physical contact [1-3]. A MG eliminates the problems associated with gear contact wear and failure caused by contact fatigue, cracking, fracturing and teeth bending fatigue [4, 5]. MGs also do not require gear lubrication and therefore removing any lubrication change costs and increases gear operating life. Coaxial MGs offer new capabilities as well, such as overload torque protection, and the potential for increased efficiency [6].

One of the main obstacles to the wide-spread use of MGs is that the torque density of the currently developed MGs is not sufficiently high to be competitive with their mechanical gearbox counterparts. For instance, mechanical gearboxes with torque densities in excess of 300 Nm/L are achievable [7, 8], while MGs to-date still struggle to break-through this limit. Fig. 1 summarizes most prior published MG volumetric torque densities that have been experimentally verified along with a number of mechanical gears from a leading gearbox manufacturer [7]. The active region volumetric torque density for each published design was computed by evaluating

$$T_v = T_p/(\pi r_{o3}^2 d) \tag{1}$$

where T_p = peak gearbox torque, r_{o3} = outer rotor radius of gear and d = active region axial length. Flux-focusing radial and axial MGs, such as studied by Uppalapati [9] and Kouhshahi [10], have been shown to be capable of achieving torque densities above 200 Nm/L. However, the flux-focusing rotor creates a rich set of higher order harmonics, and this makes it difficult to operate the MG at a high efficiency.

Halbach rotor magnet arrays are well-known for creating highly sinusoidal field distributions [11] and therefore a Halbach rotor offers the potential for both increased torque density and lower harmonic related loss. In 2009, Jian *et al.* studied the torque density and torque ripple performance of a 1:4.25 gear ratio Halbach rotor MG [12]. Jian's design achieved a peak torque and torque density of 155.8 Nm and 108 Nm/L respectively. In 2016, Jing *et al.* also constructed a 1:4.25 gear ratio Halbach rotor MG, Jing's prototype achieved a peak torque and volumetric torque density of 168 Nm and 129.8Nm/L respectively [13]. In [14] Jian convincingly demonstrated that the Halbach rotor MG could perform significantly better than the conventional radially magnetized rotor MG in terms of volumetric torque density as well as torque ripple and iron loss. Jian *et al.* [14] and Jing *et al.* [15] used 2-D analytic and 2-D finite element analysis (FEA) modeling techniques to study the performance of the Halbach PM rotor relative to the radial rotor MG equivalent and Gardner *et al.* developed a 2-D magnetic equivalent circuit model of the Halbach MG [16]. While 2-D modelling is helpful for parameter design selection the 3-D axial end-effects are particularly high within the MG [17] and therefore if the axial length is less than the radius the torque will be significantly lower than what the 2-D models predicts. This limited the torque density that could be achieved prior MG Halbach rotor designs [13]. Extensive 3-D FEA analysis is needed when trying to maximize the MG design performance [2, 18-20].

As the Halbach rotor field is focused only on one side, the Halbach rotor MG has the potential for being built with minimal steel [21, 22], for example Scheidler *et al.* [22] tested a Halbach rotor MG that utilized a 3-D printed plastic housing that attained a volumetric and mass torque density of 162 Nm/L and 44.7 N/kg respectively.

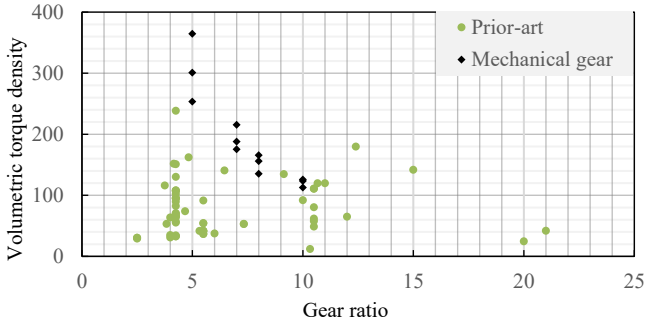

Fig. 1. Experimentally verified coaxial magnetic gear and mechanical gear active region volumetric torque density vs. gear ratio. [6, 7, 9, 12, 18, 20-55]. The mechanical gear active torque density was computed by evaluating only the mechanical gear housing region.

This work was supported by the National Science Foundation under award number 2015163 and award number 1827801.

Axial Halbach rotor MGs have also been modelled, for instance, Johnson *et al.* [56] designed an axial Halbach rotor MG that achieved a 183.9 Nm/L torque density. While the axial MG can be designed with a short stack length it is difficult to construct and maintaining the uniform airgap is challenging.

The central coaxial MG modulator is an essential element of the MG. In the past most MG designs have relied on supporting the modulator using internal support rods within the modulation segments [2], however the use of a solid conductive rod introduces significant eddy current loss. Other authors have inserted the modulator segments into a single grooved support cylinder [6, 22]. Laminated bridge supports have also been utilized both with an outer [2, 3, 39]and inner [3, 18, 38, 39, 53] and a centrally located bridge [3, 39]. Several modelling studies such as [39, 52, 53] have also been conducted that review different rectangular segment shapes [52, 57, 58]

In [55] a parametric sweep analysis was conducted for the radial configured Halbach rotor MG, this *Design A* is shown in Fig. 2, It was calculated that *Design A*, could achieve a 284N·m/L torque density and experimentally shown to reach a peak static torque density of 261 N·m/L. This paper focuses on presenting further experimental testing results for the *Design A* MG [55] as well as presenting testing and analysis results for a new Halbach MG typology that uses circular modulator rod supports. This paper shows that the use of the circular rod supports has minimal impact on the MG torque performance but greatly reduces the MG manufacturing complexity. The two circular rod designs studied in this paper are shown in Fig. 3, *Design B* use circular modulator slots with a bridge and *Design C* uses a bridgeless approach. The paper shows that the presented circular rod Halbach rotor MG design is able to achieve a volumetric torque density ≥ 280 Nm/L.

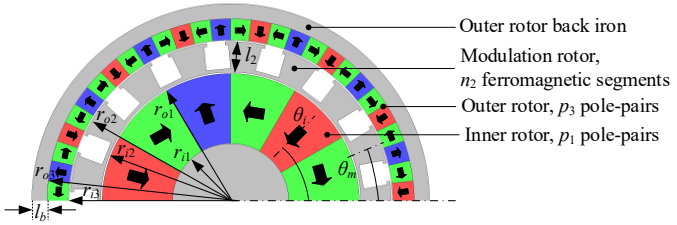

Fig. 2. A half cut-through view of the 5.67:1 gear ratio Halbach rotor MG, *Design A*. Halbach MG used rectangular modulator laminated segments.

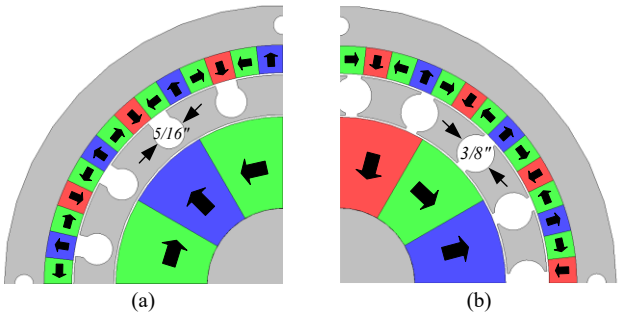

Fig. 3. Quarter view of the Halbach rotor MG with circular modulator rod supports, (a) *Design B* contains a modulator bridge and (b) *Design C* uses a bridgeless design.

II. Magnetic Design Analysis

The coaxial Halbach MG under study consisted of an inner rotor with p_1 = 3 pole-pairs, an outer rotor with p_3 = 14 pole-pairs and a ferromagnetic modulator that contained a slot number equal to $n_2 = p_1 + p_3 = 17$. With the outer rotor held fixed the torque on the inner and modulator rotor can be expressed as a sinusoidal function of the MG load angle, δ, defined as [26]

$$\delta = p_1\theta_1 - n_2\theta_2 \tag{2}$$

where θ_1 and θ_2 are the angular positions of the inner and modulator rotor as defined in Fig. 3(b). The average torque on the inner and modulator rotor is respectively

$$T_1^{avg}(\delta) = T_1'\sin(\delta) \tag{3}$$

$$T_2^{avg}(\delta) = T_2'\sin(\delta) \tag{4}$$

where the prime superscript denotes the maximum torque magnitude. With the outer rotor held fixed, and the load angle unchanged, the speed ratio is defined by [2]

$$\omega_1 = \omega_2(n_2/p_1). \tag{5}$$

giving a gear ratio $G_{12}=n_2/p_1 = 5.67$. The MG torque ripple was designed to be minimized by selecting a pole combination in which the greatest common divisor (gcd), defined as [40, 59]

$$C_T = \gcd(2p_1, n_2), \tag{6}$$

was minimized. The pole combination (p_1, n_2, p_3) = (3,17,14) gave a $C_T = 1$. It should be noted that because the modulation rotor is an odd number the radial forces on the modulation rotor are not symmetric [40]. Table I and II show the geometric MG parameters for each design, the MG radial and axial length parameters are defined in Fig. 2 and Fig. 4 respectively. All the MG designs use Nd-Fe-B, grade N48, magnet material, and the modulator was fabricated using M19 ferromagnetic laminations. The outer radius of the magnets for all the designs was r_{o3} = 60 mm and the other radial geometric parameters were selected based on the *Design A* sweep analysis, as presented in [55]. The axial length of the magnets for *Design A* was set at d = 50 mm. While the axial magnet length for *Design B* and *Design C* was set at d = 60 mm. The difference is because in [55], it was shown that an axial length of d = 50 mm was mechanically robust with respect to radial deflection so the axial length was further extended for *Design B* and *Design C*.

Maintaining a uniform modulator airgap between the inner and outer magnetic rotors is challenging because of the large radial force experienced by the ferromagnetic modulation seg-

TABLE I. Fixed Geometric and Material Parameters

Description		Value	Unit
Inner rotor	Pole pairs, p_1	3	-
	Angular span, θ_1	$\pi/(2p_1)$	radians
	Inner radius, r_{i1}	19	mm
	Outer radius, r_{o1}	42	mm
Modulation Rotor	Pole pairs, n_2	17	-
	Angular span, θ_2	π/n_2	radians
	Modulator radial length, l_2	10	mm
Outer rotor	Inner radius, r_{i3}	53	mm
	Outer radius, r_{o3}	60	mm
	Pole pairs, p_3	14	-
	Angular span, θ_3	$\pi/(2p_3)$	radians
Inner and outer rotor air gap, g		0.5	mm

ments. To minimize eddy current loss Garolite support rods were used. For the *Design A* modulation rotor, the laminations were supported using rectangular Garolite, G10, rods, as shown in Fig. 5. The rods were mechanically retained to the laminations by the small lips as shown in Fig. 2. The Garolite rods were connected to the rotor endplate on either side of the rotor using slots, as shown in Fig. 5 (c) and (d). This support structure is expensive because the Garolite rods must be custom made and the rectangular endplate slots must have a tight tolerance. In *Design B* and *Design C* the circular Garolite modulator supports were used. As the modulator radial length limit is l_2 = 10 mm, two off-the-shelf Garolite rod sizes, d_m = 6.35 mm (5/16 inch) and d_m = 9.525 mm (3/8 inch), were chosen to be studied as these diameters minimized the distortion relative to the *Design A* rectangular modulator slot.

Gerber *et al.* showed that if the modulator rotor axial length, d_c, is slightly lower than the magnet length then the torque density can be improved [17]. Based on the analysis completed in [55] the *Design A* modulator axial length was set at d_c = 47.5 mm. Repeating this analysis for *Design B* and *C* the cage modulator rotor axial length for these two designs was set at d_c = 57 mm.

The torque and torque density performance for each of the MG designs when not using a ferromagnetic back-iron is shown in Table III. The MG active region mass torque density was computed by evaluating

$$T_m = T_2'/(m_s + m_m) \tag{7}$$

where m_s = ferromagnetic modulator rotor mass and m_m = magnet material mass. *Design B* that used circular rods, with bridges, had a 6.6% lower volumetric torque density than *Design A*. The *Design C*, that did not have bridges achieved the same torque density as *Design A*, compensating the performance reduction from the circular slots.

A. Ferromagnetic Back-Iron

The *Design A* outer rotor magnets and inner rotor magnets were mechanically affixed to a ferromagnetic 1018 steel back-iron as shown in Fig. 4. The back-iron provided magnetic attraction, and assisted the magnet assembly process, however the back-iron reduces the torque. To mitigate the torque reduction the outer rotor ferromagnetic back-iron length for *Design A* was only l_b = 3mm [55]. However, to further reduce eddy current loss *Design B* and *Design C* used a ferromagnetic laminated back-iron. But to provide structural support to the outer rotor supporting rods the back-iron length needed to be radially longer. The reduction in the *Design C* peak torque when changing the outer rotor back-iron radial length, l_b, and axial length, d_b, is shown in Fig. 6. To provide sufficient rigidity a radial length of l_b = 10 mm was selected and to minimize the reduction in torque the axial length was reduced to d_b = 20mm. A summary of the 3-D FEA compute MG performance values for the three MG designs, when including the back-iron is shown in Table IV.

B. Cogging Torque Comparison

A MG has two-degrees of freedom, since the high and low speed rotors can rotate independently relative to a load angle [26]. The inner and modulator cogging torque was evaluated by subtracting the average peak torque, at $\delta = \pi/2$, from the transient FEA computed torque such that [26]

$$T_1^c(\theta_1,\delta) = T_1(\theta_1,\delta) - T_1'\sin\delta \tag{8}$$

$$T_2^c(\theta_2,\delta) = T_2(\theta_2,\delta) - T_2'\sin\delta \tag{9}$$

where superscript *c* denotes cogging torque. Fig. 7 and Fig. 8

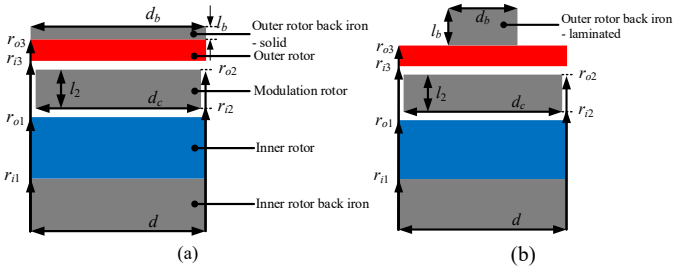

Fig. 4. Axial view of the MG defining the axial length for the modulator and outer rotor for (a) *Design A* and (b) MG *Design B* and *Design C*.

TABLE II. AXIAL LENGTH AND BACK-IRON THICKNESS VALUES

Description		***Design***			**Unit**
		A	***B***	***C***	
Modulation rotor	Axial length, d_c	47.5	57	57	mm
Outer rotor back iron	Radial thickness, l_b	3	10	10	mm
	Axial length	50	20	20	mm

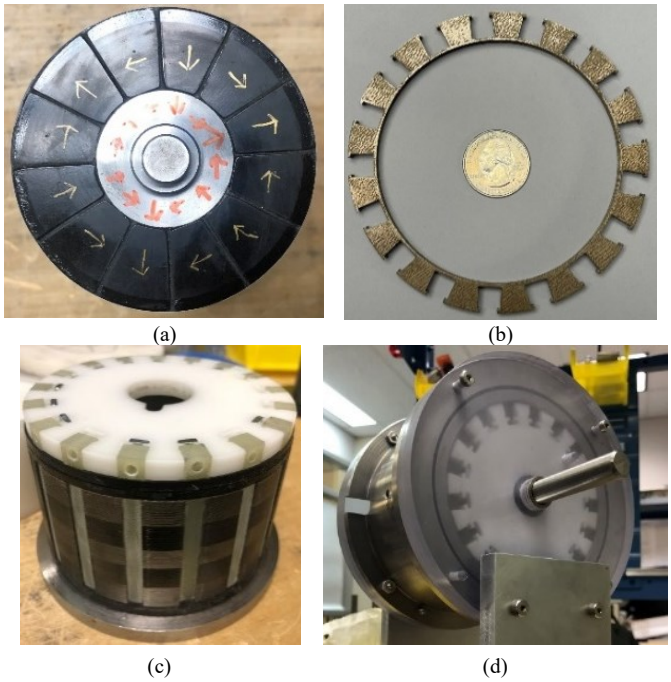

Fig. 5. (a) Inner rotor, (b) cage rotor lamination, (c) fully assembled cage rotor over the inner rotor and (d) assembled *Design A* magnetic gear [55]

TABLE III. 3-D FEA PERFORMANCE COMPARISON WITH NO OUTER ROTOR FERROMAGNETIC BACK-SUPPORT

Parameter	***Design***			**Unit**
	A	***B***	***C***	
Peak torque, T_2	160.6	180	193	Nm
Volumetric torque density, T_v	284	265.3	284.4	Nm/L
Mass torque density, T_m	43.4	40	44	Nm/kg

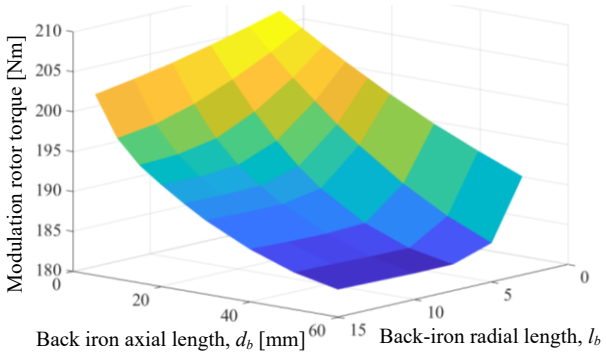

Fig. 6. *Design C* outer rotor back-iron 3-D FEA sweep analysis for the axial length and radial length

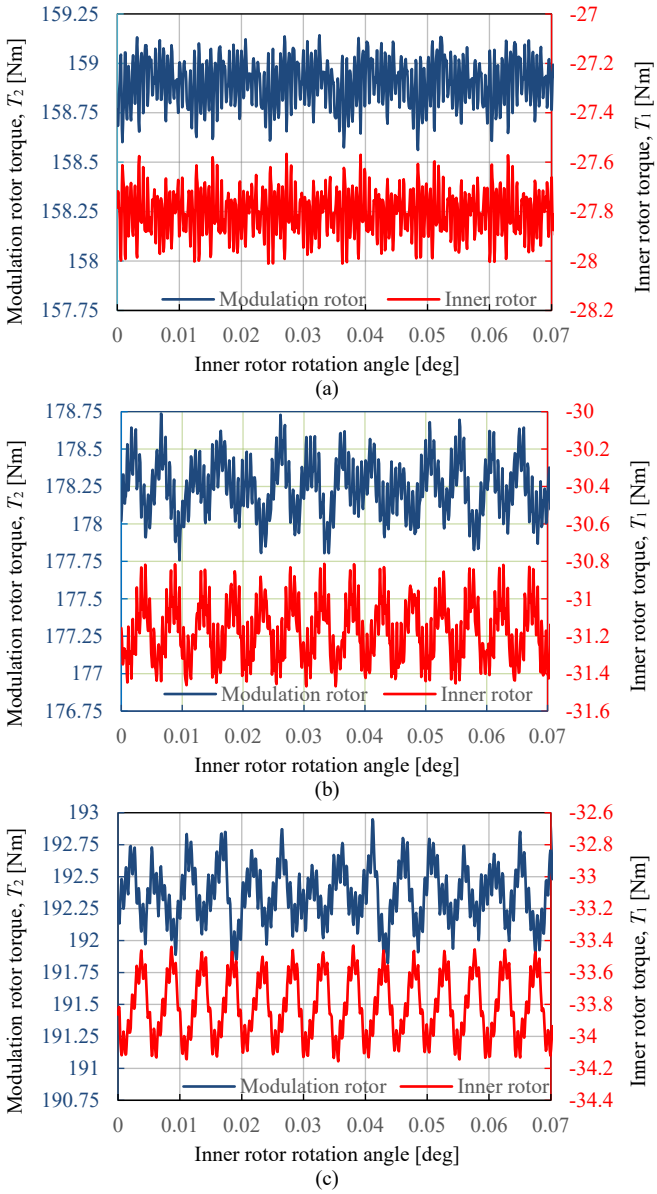

Fig. 7. 3-D FEA simulated peak-load torque ripple comparison showing torque ripple as a function of inner rotor angle for (a) *Design A*, (b) *Design B* and (c) *Design C* when losses is neglected.

TABLE IV. 3-D FEA PERFORMANCE COMPARISON

Parameter		*Design*			Unit
		A	***B***	***C***	
Peak torque, T_2		160.6	180	193	Nm
Volumetric torque density, T_p		284	265.3	284.4	Nm/L
Mass torque density, T_m		43.4	40.0	44	Nm/kg
Torque ripple at peak-load	Modulator	0.58	0.98	1.14	Nm
	Inner rotor	0.44	0.65	0.72	Nm
Percentage ripple at peak load	Modulator	0.36	0.54	0.59	%
	Inner rotor	1.58	2.08	2.12	%
Torque ripple at no-load	Modulator	0.57	0.96	1.06	Nm
	Inner rotor	0.43	0.63	0.7	Nm

shows the calculated torque ripple for the three MG designs at both peak load and no-load. Note that this FEA analysis was conducted without including loss. The modulation rotor torque at peak load for *Design B* and *Design C* is 0.54 % and 0.59 % respectively. Due to the odd number of modulation rotor slots, the torque ripple is low, but it can be seen that the use of the circular rods does increase the torque ripple magnitude. The torque ripple for the bridgeless *Design C* is only 0.05% greater than the bridged *Design B*. But *Design C* has 7.2% higher peak torque in comparison to *Design B*. Hence, the benefit of using the lamination bridge is minimal. The bridgeless circular rod *Design C* was selected to be constructed. The torque ripple for *Design C*, at no-load, is shown in Fig. 8. The no-load torque ripple for the modulation rotor and the inner rotor are 7% and 3% lower than at full load respectively.

The radial force on the one modulator segment as it rotates within the MG is shown in Fig. 9(a). This is calculated for the case when the inner and outer rotors are held stationary. Also shown in Fig. 9(b) is the total force on each modulator segment as a function of rotor position when the modulator is at zero average torque and at peak torque (peak load angle position). The odd number of modulator segments results in a non-zero radial force. It should be noted that the non-symmetric radial force and reduced noise creation within the MG can be mitigated if an even number of modulator segments are selected [36, 60].

C. Loss and Efficiency

The *Design C* steady-state eddy current loss in all rotor parts and hysteresis loss within the laminations was calculated using a transient 3-D FEA JMAG model. The fundamental frequency seen by each rotor can be calculated by evaluating [61]

$$f_1 = \frac{\omega_1}{2\pi} p_3 \tag{10}$$

$$f_2 = \frac{\omega_1}{2\pi} p_1 \frac{p_3}{n_2} \tag{11}$$

$$f_3 = \frac{\omega_1}{2\pi} p_1 \tag{12}$$

where f_1, f_2, f_3, are frequencies (in Hz) of the inner, modulation and outer rotor respectively. The modulation rotor sees the lowest electrical frequency which is calculated from (6), the loss simulation was conducted for a period of $1/f_2$ to ensure the hysteresis loss in all laminated parts reached steady state.

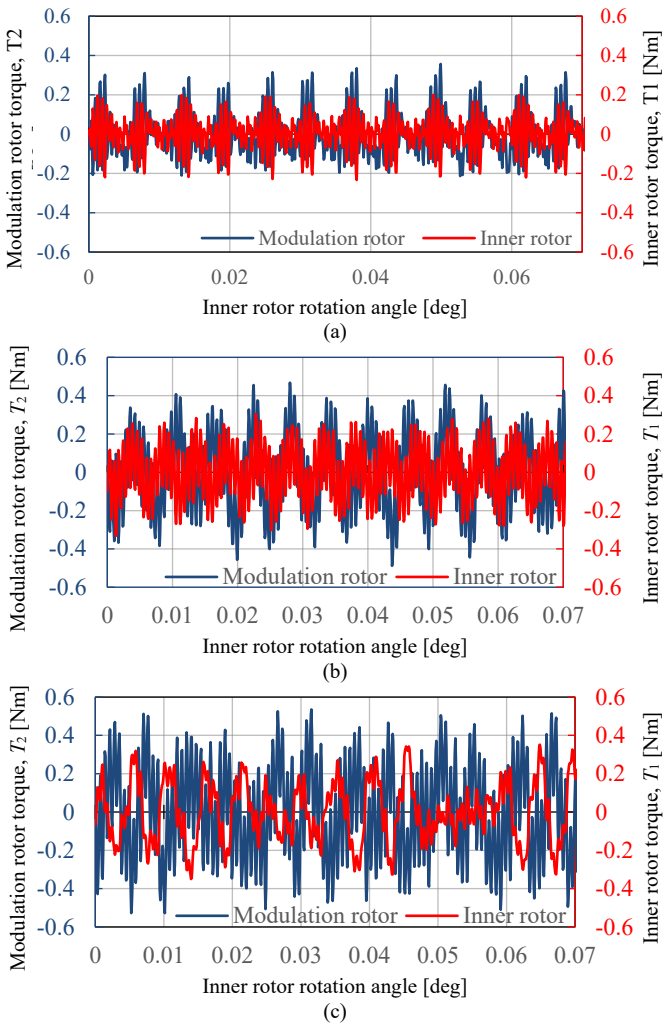

Fig. 8. 3-D FEA simulated no-load torque ripple comparison showing torque ripple as a function of inner rotor angle for (a) *Design A*, (b) *Design B* and (c) *Design C* when losses is neglected.

The power was applied on the high-speed side, when the loss is included, the power flow as a function of load angle and angular input-speed, ω_1, can be expressed as

$$T_2^{avg}(\delta,\omega_1)\cdot\omega_2 = T_1^{avg}(\delta)\cdot\omega_1 - P_l(\omega_1) \tag{13}$$

The loss within the MG can be separated into components such that

$$P_l(\omega_1) = P_e(\omega_1) + P_h(\omega_1) + P_m(\omega_1) \tag{14}$$

where P_e = eddy current losses, P_h = hysteresis losses and P_m = mechanical losses (bearings and windage). Fig. 10 shows the 3-D FEA computed no-load loss within the *Design C* MG as a function of angular speed, ω_1. The FEA computed loss has no mechanical loss component. The eddy current and hysteresis values were accurately curve fit by

$$P_e(\omega_1) = (6.96\times10^{-6})\omega_1^2 \tag{15}$$

$$P_h(\omega_1) = (5.1\times10^{-3})\omega_1 \tag{16}$$

A cross-sectional view of the FEA computed loss density within the MG at ω_1 = 1000 r/min is shown in Fig. 11. and Table V shows the break-down of loss within each component when ω_1 = 1000 r/min. Most of the loss is contained within the laminations and in the inner rotor tangentially magnetized magnets.

The loss within the MG is frequency dependent and not load dependent [21, 62]. The loss decreased the peak output torque. Rearranging (13), and noting that the gear ratio is $G_{12} = \omega_1/\omega_2$ the torque reduction as a function of the no-load loss can be determined by evaluating

$$T_2^{avg}(\delta,\omega_1) = T_1^{avg}(\delta)\cdot G_{12} - P_l(\omega_1)\frac{G_{12}}{\omega_1} \tag{17}$$

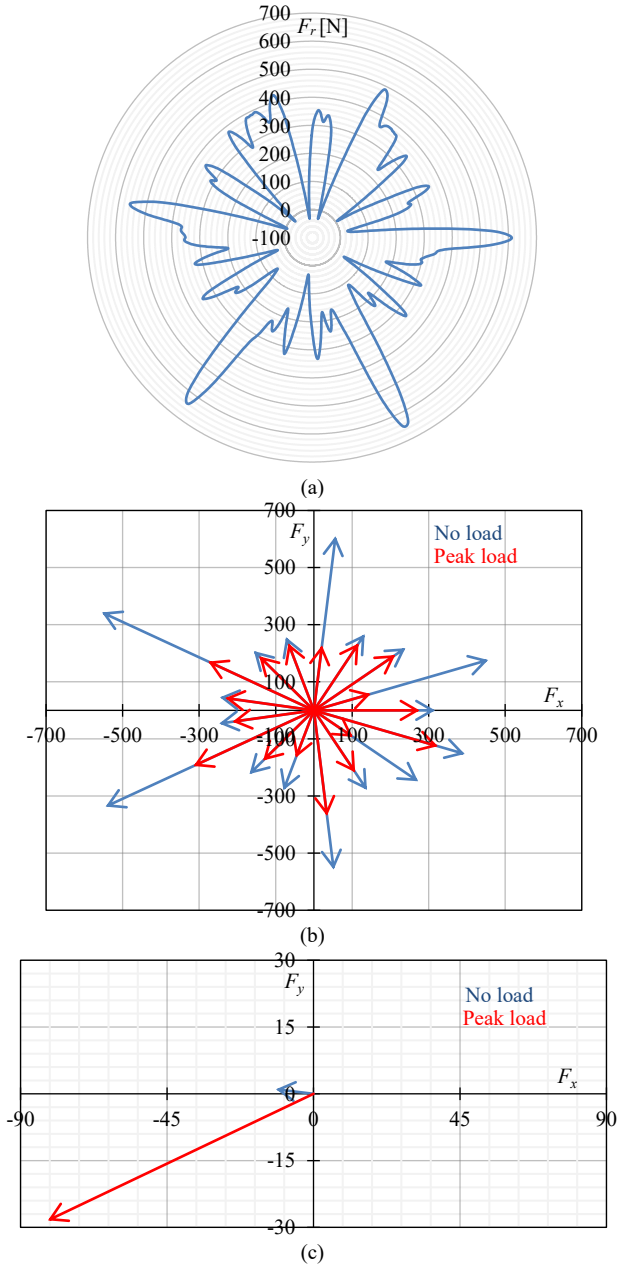

Fig. 9. Radial force, F_r, (a) as a function of angular position on one modulator segment as it is rotated. Both the inner and outer rotors were held fixed, (b) force on each of the seventeen segments at the peak and zero load angle when both rotors are stationary, and (c) net force on the entire modulation rotor at the peak and zero load angle.

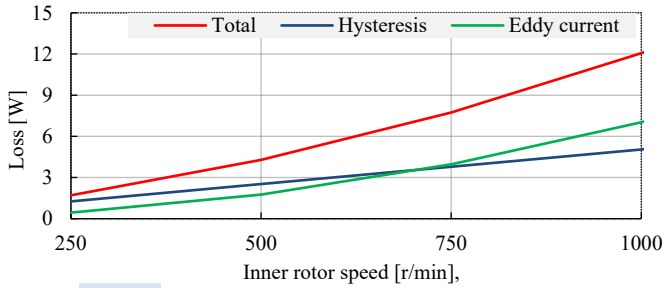

Fig. 10. *Design C* 3-D FEA calculated eddy current and hysteresis loss as a function of inner high-speed rotor speed, ω_1.

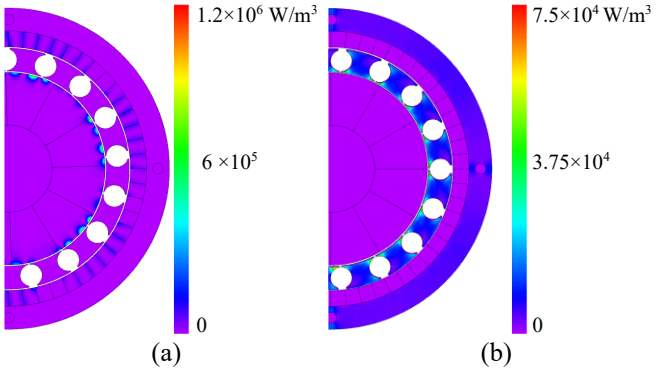

Fig. 11. (a) Joule loss density distribution within *Design C* PMs and (b) eddy current loss density within *Design C* laminations when ω_1 = 1000 r/min.

This torque reduction is small, < 0.5 Nm, because the torque reduction is only linearly proportional to the angular speed. The MG efficiency was computed by evaluating

$$\eta(\delta,\omega_1)=\frac{T_2^{avg}(\delta,\omega_1)\cdot\omega_2}{T_1^{avg}(\delta)\cdot\omega_1} \tag{18}$$

Substituting (13) into (18) gives

$$\eta(\delta,\omega_1)=1-\frac{P_l(\omega_1)}{T_1^{avg}(\delta)\cdot\omega_1} \tag{19}$$

Utilizing (19) the FEA computed efficiency map shown in Fig. 12 was created.

III. Experimental Results

The MG *Design A* was tested till failure. The peak static torque for *Design A* was measured to be T_2 = 147.8 Nm and this corresponded to a torque density of 261.4 Nm/L, this was 8 % lower than the 3-D FEA computed value.

Table VI summarizes the performance results for *Design A*. The Halbach rotor MG *Design A* failed because the inner rotor magnets disconnected from the rotor shaft steel. The reason for the failure was traced to the type of bonding glue that was selected. A misalignment on the experimental setup also resulted in a higher-than-expected torque ripple [55].

Based on the experience gained from the *Design A* testing, *Design C* used a more rigid mechanical structure and used double bearings on the low torque shaft. A cut-through view of the *Design C* prototype MG is shown in Fig. 13 and the mechanical assembly is shown in Fig. 14. Epoxy adhesive, Loctite E-40HT, was used to ensure sufficient tensile strength to secure the magnets on the surface of each rotor [20].

The experimentally measured inner and outer rotor radial magnetic fields and harmonic components for the *Design C* rotors are compared with the 3-D FEA computed values in Fig. 15 and Fig. 16 respectively. The experimental measurements were made using an AlphaLab GM2 model Gaussmeter.

The measured inner rotor magnet field fundamental component is 2.3% higher than the 3-D FEA calculated value, whereas the outer rotors fundamental component is 2.5% lower than the 3-D FEA value. After adjusting the FEA magnet material residual flux density values to match with the experimental measurements the 3-D FEA computed peak static torque reduced by 1.73 %, down to 189.7 Nm.

Fig. 17 shows the fully assembled MG on the test-stand. The high-side MG torque was measured using a Himmelstein (MCRT 48200V) torque transducer and on the low-torque side the torque was measured using a Futek (TRS300) torque transducer. An ABB DC motor (DMP132-4M) was put in torque control mode using the ABB (DCS800) drive whilst the high-speed, low-torque, side was put into speed control model

TABLE V. 3-D FEA Computed MG Component Loss at ω_1=1000 r/min

Component		Loss [W]	Loss density [W/m^3]
Inner rotor	Tangential magnets	2.56	19360.3
	Radial magnets	0.85	6428.2
	Back iron eddy current	0.05	734.8
Cage rotor	Eddy current	2.56	62371.9
	Hysteresis	3.66	
Outer rotor	Tangential magnets	0.98	13145.5
	Radial magnets	1.06	14218.6
	Back iron eddy current	0.36	21680.7
	Back iron hysteresis	1.38	
Total	Eddy current loss, P_{e1}	8.42	12727.0
	Hysteresis loss, P_{h1}	5.04	7618.1

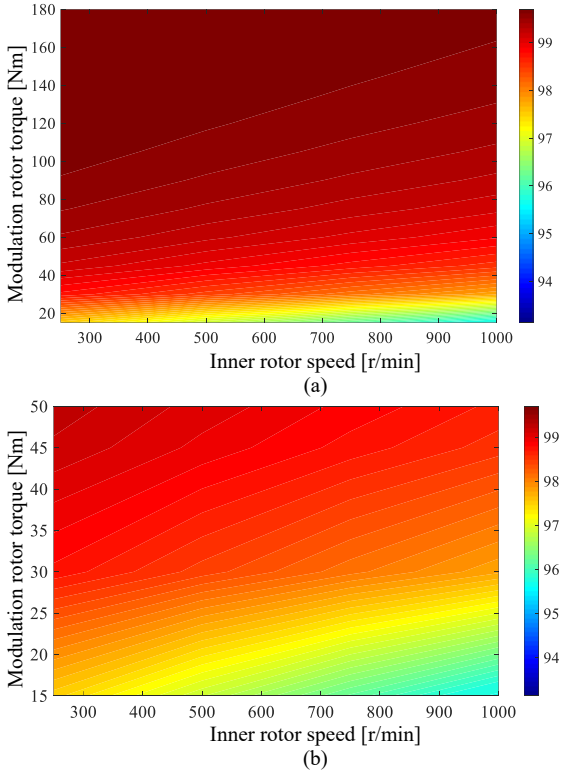

Fig. 12. (a) 3-D FEA calculated efficiency map for *Design C* with color legend indicating the efficiency and (b) a zoom-in view toward low torque level.

using the Delta-drive (C2000) and Rexroth PM-motor (MSK100C). The output power was put back onto the grid using a Delta active front-end unit (AFE2000). The static torque as a function of load angle was measured by locking the modulation rotor and rotating the inner rotor. The experimental measured torque results are shown in Fig. 18. The measured peak torque was 189.5 Nm, only a 0.5% reduction from the calculated value by the adjusted 3-D FEA model. This corresponds to an active region torque density of 279.3 Nm/L. Table VI summarizes the performance test results for the *Design C* MG.

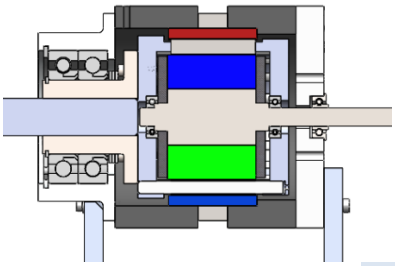

Fig. 13. Cut-through view of the mechanical assembly for *Design C*

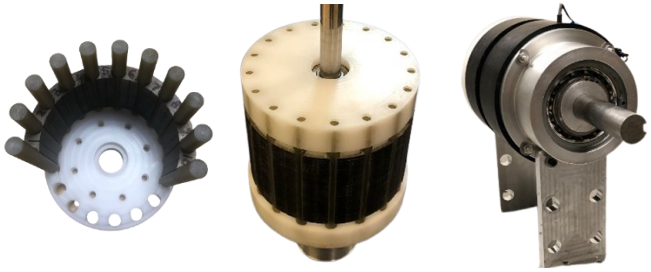

(a) (b) (c)

Fig. 14. (a) Half assembled and (b) fully assembled modulation rotor assembly, (c) fully assembled prototype outer rotor for *Design C*

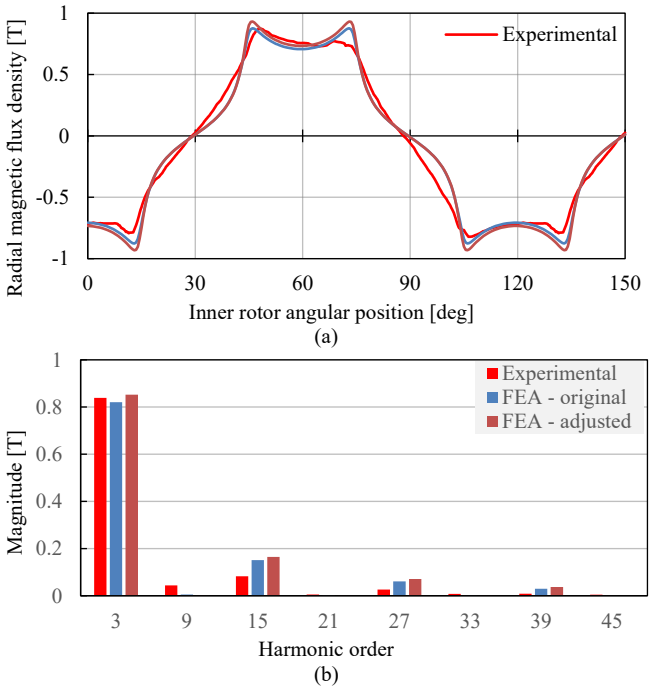

Fig. 15. 3-D FEA and experimentally measured inner rotor radial magnetic flux density field comparison for *Design C*, at (*r,* z) = (42.95, 30) mm, (b) the corresponding spatial harmonic components.

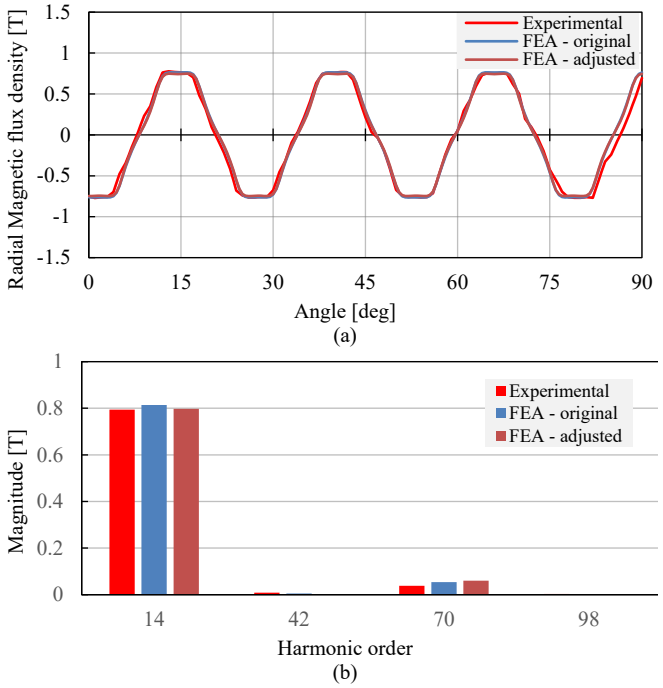

Fig. 16. 3-D FEA and experimentally measured outer rotor radial magnetic flux density field comparison for *Design C*, at (*r,* z) = (52.05, 30) mm, (b) the corresponding spatial harmonic components.

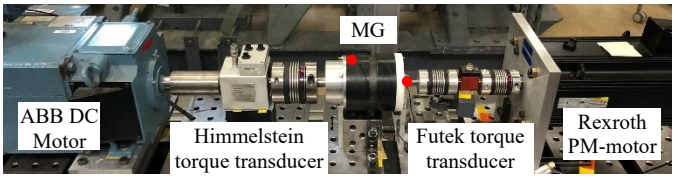

Fig. 17. The *Design C* MG test-stand, the red dots marked on the MG denote the locations of thermal couples.

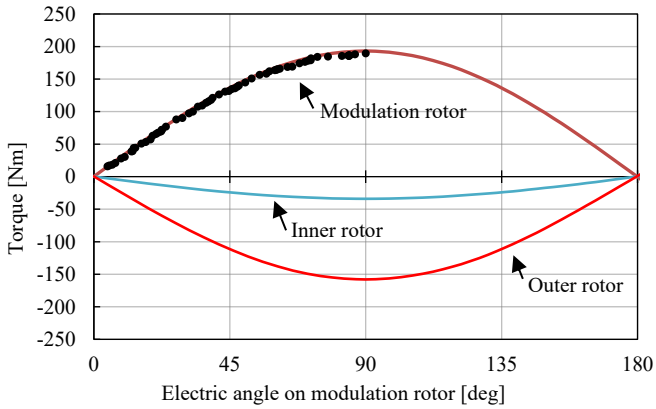

Fig. 18. *Design C* 3-D FEA static torque for as a function of electric angle. Black dots indicate the experimental measured torque at different angle.

TABLE VI. EXPERIMENTAL TEST RESULTS

Metric		*Design A*	*Design C*	Unit
Active region torque density	Peak torque	147.8	189.5	Nm
	Volumetric	261.4	279.3	Nm/L
	Mass*	39.9	43.2	Nm/kg
	Magnet mass	57.2	61.1	Nm/kg
Full assembly torque density	Volumetric	73.2	61.8	Nm/L
	Mass	22.4	19.0	Nm/kg

* Without back-iron

The load torque on the MG was stepped using the DC motor torque control and Fig. 19 shows the measured MG torque at different load torque values as a function of time for the case when the inner rotor angular speed is ω_1 = 1000 r/min. The torque ripple was measured by operating the MG with the load motor turned off but still mechanically connected. Fig. 20 shows the measured no-load torque and peak-load torque ripple. A comparison between the measured and FEA calculated torque ripple metrics at both the non-load and peak torque angle is shown in shown in Table VII.

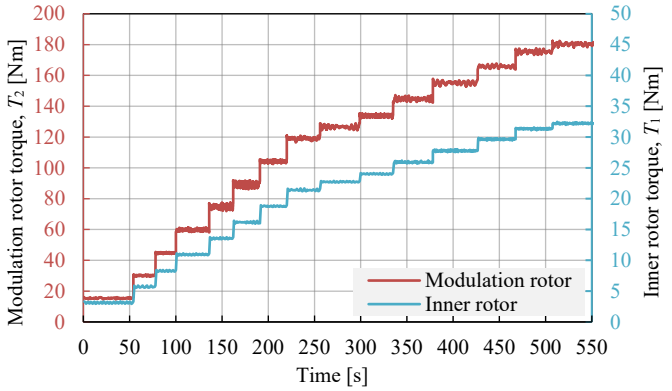

Fig. 19. *Design C* Measured torque with applied 1000 r/min on the high-speed rotor and changing load on the low-speed rotor.

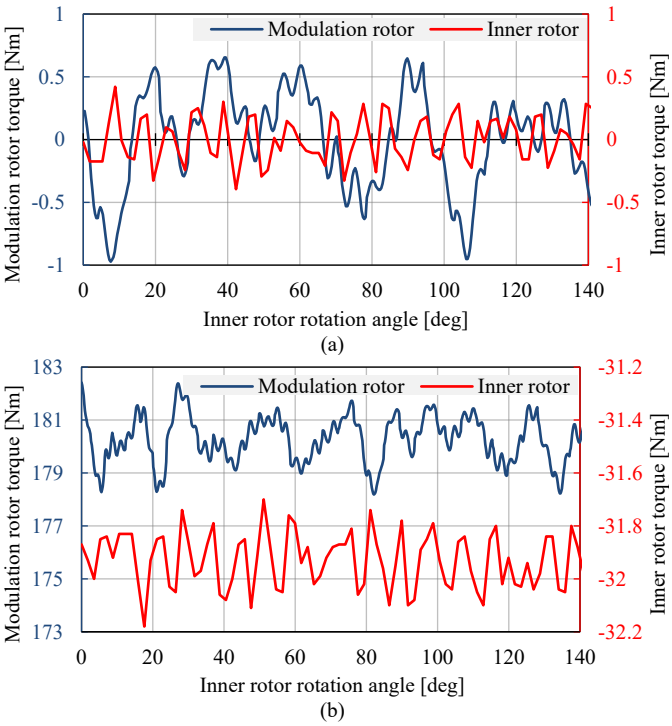

Fig. 20. Experimentally measured *Design C* MG modulator torque and inner rotor torque at (a) no-load and (b) peak-load when the inner rotor angular speed is ω_1 = 250 r/min.

TABLE VII. TORQUE RIPPLE COMPARISON BETWEEN 3-D FEA CALCULATION AND EXPERIMENTAL MEASUREMENTS

Metric		3-D FEA	Experimental	**% Error**
Inner rotor	No-load	0.7	0.82	17.1%
	Peak load	0.72	0.48	-33.3%
Modulation rotor	No-load	1.06	1.63	53.8%
	Peak load	1.14	4.23	271.1%

The discrepancy between the measurement and calculated will be in part due to the additional torque ripple sourced from the two motors on the experimental setup as well as the inclusion of losses in the experimentally measured torque ripple plot. The experimental measured loss at ω_1 = 1000 r/min is shown in Fig. 21, unfortunately it is 246 % higher than the calculated loss. The measured loss is accurately described by:

$$P_l(\omega_1) = (40\times10^{-6})\omega_1^2 + (1.3\times10^{-3})\omega_1 \qquad (20)$$

At ω_1 =1000 r/min loss attributed to the eddy currents ω_1^2 term is 5.7 time higher than computed. While the measured loss associated with the linear speed term is 3.9 times lower than expected. The higher loss is likely caused by the neglecting the in-plane eddy current loss [63].

Substituting (20) into (19) gives the efficiency contour plot as shown in Fig. 22. Despite the increased loss the efficiency near the peak torque reached above 98%.

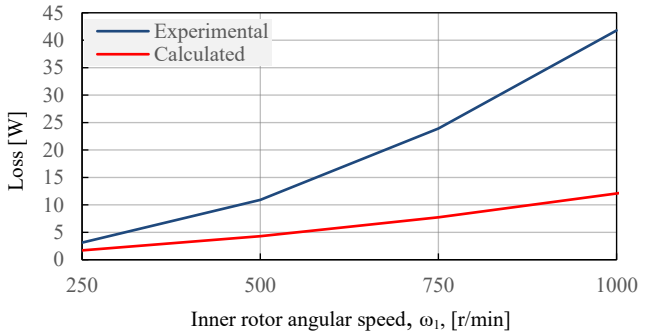

Fig. 21. Comparison plot between 3-D FEA calculated loss and experimentally measured *Design C* loss as a function of angular speed when T_2 = 180 Nm.

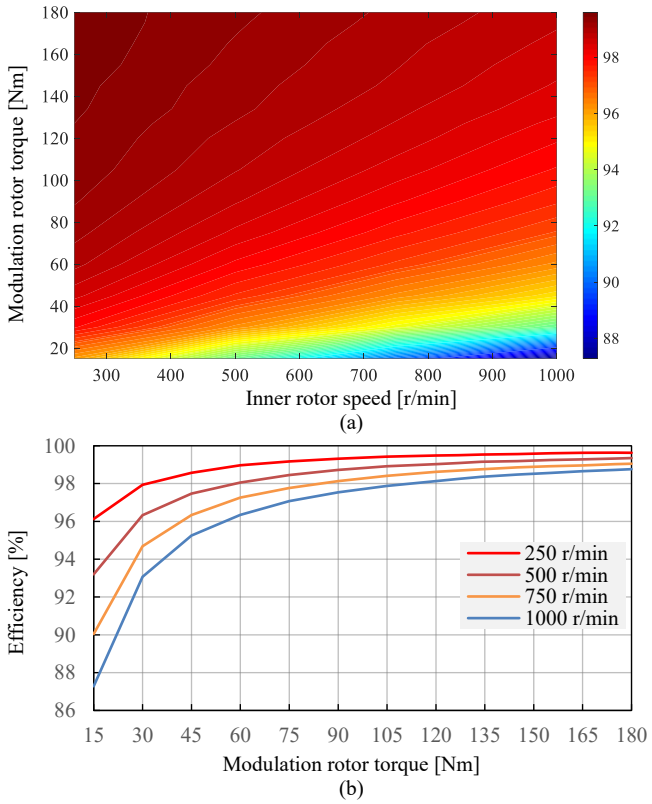

Fig. 22. (a) *Design C* Efficiency map using eddy current loss curve fit values. (b) experimentally measured efficiency vs modulation rotor torque.

A. *Thermal Analysis*

A thermal analysis of the MG was performed using an ANSYS 3-D finite element analysis thermal conduction model [64] The component loss density within the MG as a function of time was computed at ω_1 = 250 r/min angular speed step increments and a steady-state thermal analysis was then computed by using the loss values as heat source elements. The thermal model used the heat transfer coefficient values as shown in Table VIII.

The outside MG temperature was measured using a FLIR (E6390) thermal camera. Fig. 23 shows a comparison between the FEA calculated temperature change at ω_1 = 2000 r/min. Table IX summarizes the maximum temperature calculated on the different components at each angular speed and Fig. 24 shows the comparison between the FEA calculated and experimentally measured torque on the outer rotor laminations. When at ω_1 = 2000 r/min the conservative thermal FEA model, predicted a 22.1 % higher temperature than the measured value.

II. Conclusion

This paper has presented the design, analysis, and experimental testing results for a high torque density Halbach rotor coaxial MG. Both a rectangular and circular modulator rod support design was tested. The new circulator modulator rod support MG design was shown to be capable of achieving a competitive torque density performance relative to a mechanical gear equivalent whilst also operating with a low torque ripple. The bridgeless circular rod modulator design was experimentally measured to be capable of operating at a peak torque and torque density of 189.5 Nm and 279.3 Nm/L respectively. The authors believe that this presented coaxial MG has attained the highest published active region torque density.

TABLE VIII. HEAT TRANSFER COEFFICIENTS

Region	Value [W/m·K]
Airgap areas	0.026
Garolite support rods and rotor end plates	0.3
Cage rotor and outer rotor laminations [65]	28
Nd-Fe-B magnets	7.6
Aluminum end plates	230
Rotor shafts and inner back iron (1018 steel)	51.9

TABLE IX. MAXIMUM TEMPERATURE CALCULATED ON DIFFERENT MG PARTS AT DIFFERENT SPEED ON VERSION 2 MG

Ambient Temp 22 ºC		Temperature [ºC]				
		Inner magnets	Outer magnets	Modulation rotor lamination	Outer lamination	Inner back iron
Inner rotor speed [r/min]	250	29.5	27	35.1	27	29.5
	500	34.3	29.8	41.9	29.8	34.2
	750	41.6	33.7	51.6	33.7	41.6
	1000	51.8	38.6	61.7	38.6	51.7
	1250	64.5	44.6	73.1	44.6	64.3
	1500	79.9	51.5	85.8	51.5	79.5
	1750	97.8	59.5	99.8	59.5	97.3
	2000	118.3	68.6	115	68.5	117.7

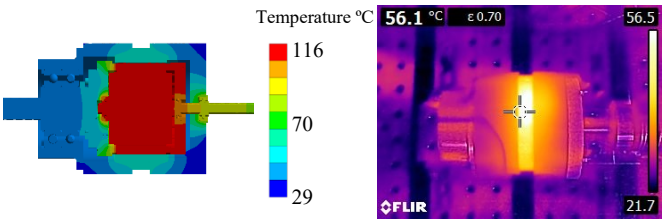

Sectional view of ANSYS thermal FEA calculated temperature contour plot (a)

Thermal camera image (b)

Fig. 23 Image of (a) FEA calculated temperature and (b) thermal camera taken at ω_1 = 2000 r/min.

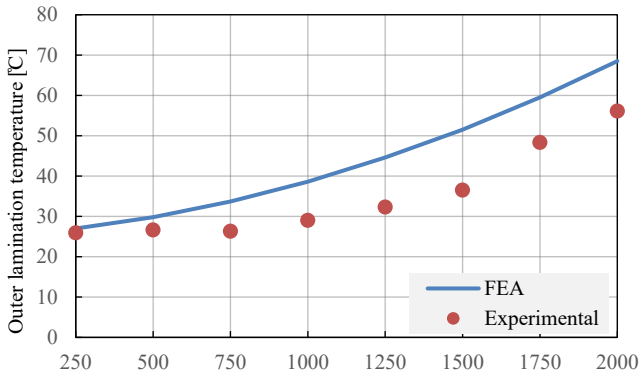

Fig. 24 Outer lamination temperature comparison between the FEA calculated and experimental measured at different inner rotor speeds.

III. Acknowledgements

The authors would like to thank the JMAG and ANSYS Corporations for the use of their FEA software.

IV. References

[1] T. B. Martin, "Magnetic Transmission," USA Patent 3,378,710, 1968.

[2] K. Atallah, S. D. Calverley, and D. Howe, "Design, analysis and realisation of a high-performance magnetic gear," *IEE Proc.-Electr. Power Appl.,* vol. 151, no. 2, pp. 135-143, 2004.

[3] B. Ackermann and L. Honds, "Magnetic drive arrangement comprising a plurality of magnetically cooperating parts which are movable relative to one another," U.S. Patent 5,633,555, 1997.

[4] A. R. Nejad, Z. Gao, and O. Moan, "Fatigue Reliability-Based Inspection and Maintenance Planning of Gearbox Components in Wind Turbine Drivetrains," *Energy Procedia* vol. 53, pp. 248 – 257, 2014.

[5] Shuangwen Sheng, M. McDade, and R. Errichello, "Wind Turbine Gearbox Failure Modes - A Brief (Presentation)," presented at the ASME/STLE 2011 Int. Joint Tribology Conf., Los Angeles, California, Oct. 24-26,, 2011.

[6] P. O. Rasmussen, T. O. Andersen, F. T. Jorgensen, and O. Nielsen, "Development of a high-performance magnetic gear," *IEEE Trans. Ind. Appl.,* vol. 41, no. 3, pp. 764-770, 2005.

[7] Neugart. https://www.neugart.com/en/

[8] "Sm-Cyclo Speed Reducers and Gearmotorsed: Series 4000." Sumitomo Machinary Corporation of America. (accessed.

[9] K. K. Uppalapati, J. Z. Bird, J. Wright, J. Pitchard, M. Calvin, and W. Williams, "A magnetic gearbox with an active region torque density of 239Nm/L," *IEEE Trans. Ind. Appl.,* vol. 54, no. 2, pp. 1331-1338, April 2018.

[10] M. Bahrami Kouhshahi, V. M. Acharya, M. Calvin, J. Z. Bird, and W. Williams, "Designing and experimentally testing a flux-focusing axial flux magnetic gear for an ocean generator application," *IET Electric Power Appl.,* vol. 13, no. 8, pp. 1212-1218, 2019.

[11] K. Halbach, "Design of permanent multipole magnets with oriented rare earth cobalt material," *Nuclear Instruments and Methods,* vol. 169, no. 1, pp. 1-10, 1980.

[12] L. Jian, K. T. Chau, Y. Gong, J. Z. Jiang, C. Yu, and W. Li, "Comparison of Coaxial Magnetic Gears With Different Topologies," *IEEE Trans. on Magn.,* vol. 45, no. 10, pp. 4526-4529, 2009.

[13] L. Jing, L. Liu, Y. Zhang, and J. Su, "Parameters analysis and optimization design for concentric magnetic gear with halbach permanent-magnet arrays," (in Chinese), *EMC,* vol. 20, no. 3, 2016.

[14] L. Jian and K. T. Chau, "A Coaxial Magnetic Gear With Halbach Permanent-Magnet Arrays," *IEEE Trans. on Energy Conv.,* vol. 25, no. 2, pp. 319-328, 2010.

[15] L. B. Jing and Y. J. Zhang, "Exact analytical method for magnetic field computation in the concentric magnetic gear with Halbach permanent-magnet arrays," in *IEEE Int. Conf. on Applied Supercond. and Electromagn. Devices*, Oct. 2013, pp. 343-346.

[16] M. C. Gardner, D. A. Janak, and H. A. Toliyat, "A Parameterized Linear Magnetic Equivalent Circuit for Air Core Radial Flux Coaxial Magnetic Gears with Halbach Arrays," in *IEEE Energy Conv. Cong. and Expo. (ECCE)*, 23-27 Sept. 2018, pp. 2351-2358.

[17] S. Gerber and R. Wang, "Analysis of the end-effects in magnetic gears and magnetically geared machines," in *Int.l Conf. on Elect. Mach. (ICEM)*, 2-5 Sept. 2014, pp. 396-402.

[18] S. Gerber and R. Wang, "Evaluation of a prototype magnetic gear," in *IEEE Int. Conf. on Ind. Tech. (ICIT)*, Feb. 2013, pp. 319-324.

[19] M. C. Gardner, B. E. Jack, M. Johnson, and H. A. Toliyat, "Comparison of Surface Mounted Permanent Magnet Coaxial Radial Flux Magnetic Gears Independently Optimized for Volume, Cost, and Mass," *IEEE Trans. on Industry Appl.,* vol. 54, no. 3, pp. 2237-2245, 2018.

[20] H. Y. Wong, H. Baninajar, B. Dechant, and J. Bird, "Designing a Magnetic Gear for an Electric Aircraft Drivetrain," in *IEEE Energy Conv. Cong. and Expo. (ECCE)*, Oct. 2020, pp. 1-6.

[21] M. C. Gardner, M. Johnson, and H. A. Toliyat, "Performance Impacts of Practical Fabrication Tradeoffs for a Radial Flux Coaxial Magnetic Gear with Halbach Arrays and Air Cores," in *IEEE Energy Conv. Cong. and Expo. (ECCE)*, 2019, pp. 3129-3136.

[22] J. J. Scheidler, V. M. Asnani, and T. F. Tallerico, "NASA's Magnetic Gearing Research for Electrified Aircraft Propulsion," in *AIAA/IEEE Electric Aircraft Tech. Sympo. (EATS)*, July 2018, pp. 1-12.

[23] D. Som, K. Li, J. Kadel, J. Wright, S. Modaresahmadi, J. Z. Bird, and W. William, "Analysis and Testing of a Coaxial Magnetic Gearbox With Flux Concentration Halbach Rotors," *IEEE Trans. on Magn.,* vol. 53, no. 11, pp. 1-6, 2017.

[24] N. W. Frank and H. A. Toliyat, "Analysis of the Concentric Planetary Magnetic Gear With Strengthened Stator and Interior Permanent Magnet Inner Rotor," *IEEE Trans. on Ind. App.,* vol. 47, no. 4, pp. 1652-1660, 2011.

[25] N. Niguchi and K. Hirata, "Cogging Torque Analysis of Magnetic Gear," *IEEE Trans. on Ind. Electr.,* vol. 59, no. 5, pp. 2189-2197, 2012.

[26] S. Gerber and R. Wang, "Cogging Torque Definitions for Magnetic Gears and Magnetically Geared Electrical Machines," *IEEE Trans. on Magn.,* vol. 54, no. 4, pp. 1-9, 2018.

[27] S. S. Nielsen, R. K. Holm, and P. O. Rasmussen, "Conveyor System With a Highly Integrated Permanent Magnet Gear and Motor," *IEEE Trans. on Industry Appl.,* vol. 56, no. 3, pp. 2550-2559, 2020.

[28] X. Liu, K. T. Chau, J. Z. Jiang, and C. Yu, "Design and analysis of interior-magnet outer-rotor concentric magnetic gears," *Journal of Applied Physics,* vol. 105, no. 7, p. 07F101, April 2009.

[29] K. Li, S. Modaresahmadi, W. B. Williams, J. D. Wright, D. Som, and J. Z. Bird, "Designing and Experimentally Testing a Magnetic Gearbox for a Wind Turbine Demonstrator," *IEEE Trans. on Ind. Appl.,* vol. 55, no. 4, pp. 3522-3533, 2019.

[30] L. Bronn, R.-J. Wang, and M. Kamper, "Development of a shutter type magnetic gear," presented at the Southern African Univ. Power Engine. Conf., Johannesburg, 2010.

[31] T. F. T. Z. A. C. Justin J. Scheidler, "Dynamic Testing of a High-Specific-Torque Concentric Magnetic Gear," *IEEJ Trans. on Ind. Appl.,* vol. Annual Forum & Technology Display - The Future of Vertical Flight, 2019/05/13/ 2019.

[32] K. Li, S. Modaresahmadi, W. B. Williams, J. Z. Bird, J. D. Wright, and D. Barnett, "Electromagnetic Analysis and Experimental Testing of a Flux Focusing Wind Turbine Magnetic Gearbox," *IEEE Trans. on Energy Conv.,* vol. 34, no. 3, pp. 1512-1521, 2019.

[33] A. Matthee, R.-J. Wang, C. Agenbach, D. Els, and M. Kamper, "Evaluation of a Magnetic Gear for Air-Cooled Condenser Applications," *IET Electric Power Appl.,* vol. 12, pp. 677-683, 05/01 2018.

[34] K. K. Uppalapati, W. B. Bomela, J. Z. Bird, M. D. Calvin, and J. D. Wright, "Experimental Evaluation of Low-Speed Flux-Focusing Magnetic Gearboxes," *IEEE Trans. on Industry Appl.,* vol. 50, no. 6, pp. 3637-3643, 2014.

[35] M. Fukuoka, K. Nakamura, and O. Ichinokura, "Experimental tests of surface permanent magnet magnetic gear," in *Int. Conf. on Elect. Mach. and Syst. (ICEMS)*, Oct. 2012, pp. 1-6.

[36] C. J. Agenbach, D. N. J. Els, R. J. Wang, and S. Gerber, "Force and Vibration Analysis of Magnetic Gears," 2018, pp. 752-758.

[37] A. Matthee, S. Gerber, and R.-J. Wang, "A high performance concentric magnetic gear," presented at the Southern African Univ. Power Engine. Conf., Johannesburg, 2015.

[38] M. Kowol, J. Kołodziej, M. Jagieła, and M. Łukaniszyn, "Impact of Modulator Designs and Materials on Efficiency and Losses in Radial Passive Magnetic Gear," *IEEE Trans. on Energy Conv.,* vol. 34, no. 1, pp. 147-154, 2019.

[39] K. Li, K. Uppalapati, J. Wright, J. Kadel, J. Z. Bird, and W. Willimas, "Investigating the Performance of a Fully Laminated Flux-Focusing Magnetic Gearbox," *Progress In Electromagn. Res. Conv.,* vol. 87, pp. 51-62, 01/01 2018.

[40] G. Jungmayr, J. Loeffler, B. Winter, F. Jeske, and W. Amrhein, "Magnetic Gear: Radial Force, Cogging Torque, Skewing, and Optimization," *IEEE Trans. on Industry Appl.,* vol. 52, no. 5, pp. 3822-3830, 2016.

[41] J. S. V. Asnani, and T. Tallerico, "Magnetic gearing research at NASA.," presented at the AHS International 74th Annual Forum & Technology Display, Phoenix, Arizona, 2018.

[42] J. L. PerezDiaz, E. DiezJimenez, C. Cristache, I. ValienteBlanco, M. AlvarezValenzuela, V. Castro, E. RuizNavas, J. Sánchez García Casarrubios, C. Ferdeghini, F. Canepa, W. Hornig, G. Carbone, J. Plechacek, A. Amorin, J. Serrano, and V. Sanz, "Magnetic Non-Contact Harmonic Drive," in *ASME Int. Mech. Eng. Cong. and Expo. (IMECE), Proceedings* 2013, vol. 1,

[43] S. S. Nielsen, R. K. Holm, N. I. Berg, and P. O. Rasmussen, "Magnetically geared conveyor drive unit - an updated version," in *IEEE Energy Conv. Cong. and Expo. (ECCE)*, Oct 2020, pp. 285-292.

[44] L. Jian, Z. Deng, Y. Shi, J. Wei, and C. C. Chan, "The Mechanism How Coaxial Magnetic Gear Transmits Magnetic Torques Between Its Two Rotors: Detailed Analysis of Torque Distribution on Modulating Ring," *IEEE/ASME Trans. on Mechatronics,* vol. 24, no. 2, pp. 763-773, 2019.

[45] R. Zanis, A. Borisavljevic, J. W. Jansen, and E. A. Lomonova, "Modeling, design and experimental validation of a small-sized magnetic gear," 2013, pp. 560-565.

[46] M. Kowol, J. Kołodziej, R. Gabor, M. Lukaniszyn, and M. Jagiela, "On-Load Characteristics of Local and Global Forces in Co-Axial Magnetic Gear with Reference to Additively Manufactured Parts of Modulator," *Energies,* vol. 13, p. 3169, 06/18 2020.

[47] J. EsnozLarraya, I. ValienteBlanco, C. Cristache, J. Sánchez García Casarrubios, F. RodriguezCelis, E. DiezJimenez, and J. L. PerezDiaz, *OPTIMAGDRIVE: High Perf Mag. Gears Dev. for Space Appl.* 2017.

[48] N. Iwasaki, M. Kitamura, and Y. Enomoto, "Optimal Design of Permanent Magnet Motor with Magnetic Gear and Prototype Verification," *Ieej Trans. on Ind. Appl.,* vol. 134, pp. 439-446, 04/01 2014.

[49] L. Jing, L. Liu, M. Xiong, and D. Feng, "Parameters Analysis and Optimization Design for a Concentric Magnetic Gear Based on Sinusoidal Magnetizations," *IEEE Trans. on Applied Supercond.,* vol. 24, no. 5, pp. 1-5, 2014.

[50] K. K. Uppalapati, J. Z. Bird, D. Jia, J. Garner, and A. Zhou, "Performance of a magnetic gear using ferrite magnets for low speed ocean power generation," 2012, pp. 3348-3355.

[51] J. L. Perez-Diaz, E. Diez-Jimenez, I. Valiente-Blanco, C. Cristache, M. Alvarez-Valenzuela, J. Sánchez García Casarrubios, C. Ferdeghini, F. Canepa, W. Hornig, G. Carbone, J. Plechacek, A. Amorim, T. Frederico, P. Gordo, J. Abreu, V. Sanz, E. Ruiz-Navas, and J. Martínez Rojas, "Performance of Magnetic-Superconductor Non-Contact Harmonic

Drive for Cryogenic Space Applications," *Machines,* vol. 2015, pp. 138-156, July 2015.

[52] T. Fujita, Y. Ando, K. Nagaya, M. Oka, T. Todaka, M. Enokizono, and K. Sugiura, "Surface Magnet Gears with a New Magnet Arrangement and Optimal Shape of Stationary Pole Pieces," *Journal of Electromagn.Analy. and Appl.,* vol. 5, pp. 243-249, 01/01 2013.

[53] N. Niguchi, K. Hirata, M. Muramatsu, and Y. Hayakawa, "Transmission torque characteristics in a magnetic gear," in *The XIX Int. Conf. on Elect. Mach. - ICEM*, Sept. 2010, pp. 1-6.

[54] L. Shah, A. Cruden, and B. W. Williams, "A Variable Speed Magnetic Gear Box Using Contra-Rotating Input Shafts," *IEEE Trans. on Magn.,* vol. 47, no. 2, pp. 431-438, 2011.

[55] H. Y. Wong, J. Z. Bird, D. Barnett, and W. William, "A High Torque Density Halbach Rotor Coaxial Magnetic Gear," presented at the IEEE Intern. Electric Mach. Drives Conf. , San Diego, CA, USA, 2019.

[56] M. Johnson, M. C. Gardner, and H. A. Toliyat, "Analysis of axial field magnetic gears with Halbach arrays," in *IEEE Int. Elect. Mach. & Drives Conf. (IEMDC)*, May 2015, pp. 108-114.

[57] X. Li, S. Liu, Y. Wang, and Y. Fan, "Investigation of the flux leakage effects in transverse-flux magnetic gear," in *Int. Conf. on Elect.l Mach. and Syst. (ICEMS)*, 2017, pp. 1-5.

[58] D. K. Jang and J. H. Chang, "Effect of Stationary Pole Pieces with Bridges on Electromagnetic and Mechanical Performance of a Coaxial Magnetic Gear," *Journal of Magn.,* vol. 18, 06/30 2013.

[59] Z. Q. Zhu and D. Howe, "Influence of design parameters on cogging torque in permanent magnet machines," in *IEEE Int. Elec. Mach. and Drives Conf. Record*, May 1997, pp. MA1/3.1-MA1/3.3.

[60] S. S. Nielsen, H. Y. Wong, H. Baninajar, J. Z. Bird, and P. O. Rasmussen, "Pole and Segment Combination in Concentric Magnetic Gears: Vibrations and Acoustic Signature," *IEEE Transactions on Energy Conversion,* pp. 1-1, 2022.

[61] M. Filippini, P. Alotto, V. Cirimele, M. Repetto, C. Ragusa, L. Dimauro, and E. Bonisoli, "Magnetic Loss Analysis in Coaxial Magnetic Gears," *Electronics,* vol. 8, no. 11, 2019.

[62] M. Fukuoka, K. Nakamura, and O. Ichinokura, "Experimental Tests and Efficiency Improvement of Surface Permanent Magnet Magnetic Gear," *IEEJ Journal of Ind. Appl.,* vol. 3, no. 1, pp. 62-67, 2014.

[63] H. Baninajar, S. Modaresahmadi, H. Y. Wong, J. Z. Bird, W. Williams, B. Dechant, and P. Southwick, "A Dual-Stack Coaxial Magnetic Gear for a Marine Hydrokinetic Generator Application," *submitting to IEEE Trans. on Energy Conv. ,* 2022.

[64] S. Modaresahmadi, J. Khalesi, K. Li, J. Z. Bird, and W. B. Williams, "Convective heat transfer analysis of a laminated flux focusing magnetic gearbox," *Thermal Science and Engineering Progress,* vol. 18, p. 100552, Aug 2020.

[65] J. F. Gieras, "Material engineering," in *Advancements in Electric Machines*. Dordrecht: Springer Netherlands, 2008, p. 29.